

Nucleon Energy Correlators for the Color Glass Condensate

Hao-Yu Liu,¹ Xiaohui Liu,^{1,*} Ji-Chen Pan,² Feng Yuan,^{3,†} and Hua Xing Zhu^{4,‡}

¹*Center of Advanced Quantum Studies, Department of Physics,
Beijing Normal University, Beijing, 100875, China*

²*Institute of High Energy Physics and School of Physics,
Chinese Academy of Sciences, Beijing 100049, China*

³*Nuclear Science Division, Lawrence Berkeley National Laboratory, Berkeley, CA 94720, USA*

⁴*Zhejiang Institute of Modern Physics, Department of Physics, Zhejiang University, Hangzhou, 310027, China*

We demonstrate the recently proposed nucleon energy-energy correlator (nucleon EEC) $f_{\text{EEC}}(x, \theta)$ can unveil the gluon saturation in the small- x regime in eA collisions. The novelty of this probe is that it is fully inclusive just like the deep-inelastic scattering (DIS), with no requirements of jets or hadrons, but still provides an evident portal to the small- x dynamics through the shape of the θ -distribution. We find that the saturation prediction is significantly different from the expectation of the collinear factorization.

Introduction. Small- x gluon saturation [1–6] has been one of the central focuses in nuclear physics community in recent years and will be a major research area in the future Electron Ion Collider (EIC) [7–9]. An effective field theory called color-glass-condensate (CGC) [4–6] has been established to compute the hadronic and nuclear structure functions in deep inelastic scattering (DIS) at small values of Bjorken- x_B [10, 11]. The CGC predicts the gluon saturation with a characteristic scale Q_s , as a consequence of the small- x nonlinear dynamics governed by the BK-JIMWLK equation [12–17]. The saturation scale Q_s represents the typical size of the gluon transverse momentum inside the nucleus and grows as the momentum fraction $x \rightarrow 0$. For large nucleus and small- x , typically $Q_s > \Lambda_{\text{QCD}}$.

Previous experiments from DIS in ep collisions at HERA and hadron productions in pA collisions at RHIC and LHC have shown some evidence of gluon saturation at small- x . With the planned EIC in the horizon, this physics will be explored in a systematic manner with unprecedented precision [7–9]. Extensive studies have been carried out for the EIC experiments, including the inclusive DIS structure functions at small- x_B [18–20] and the azimuthal correlations of di-jet/di-hadron/photon-jet/lepton-jet in the inclusive or diffractive processes [21–56]. These processes are considered as promising channels to look for the gluon saturation in eA collisions.

In this manuscript, we present a novel approach to probe the gluon saturation in eA collisions in terms of the nucleon energy-energy correlator (nucleon EEC) recently proposed in Ref. [57], which is an extension of the EEC [58, 59] to the nucleon case. The EEC is the vacuum expectation of a set of final state correlators to reformulate jet substructures [60–84], while the nucleon EEC is the nucleon expectation of the initial-final state correlator. The latter encodes the partonic angular distribution induced by the intrinsic transverse momentum within the nucleon [57]. Therefore we expect the features of the gluon saturation, especially the saturation scale Q_s that measures the size of the intrinsic trans-

verse momentum, should be naturally imprinted in the nucleon EEC. Our numeric results in Figs. 5 and 6 will show that the saturation predictions have distinguished behaviors as compared to those from the collinear factorization. From this comparison, we can further deduce the saturation scales in ep and eA collisions, respectively.

The quark contribution to the nucleon EEC in the momentum space is defined as

$$f_{q,\text{EEC}}(x, \theta) = \int \frac{dy^-}{4\pi E_A} e^{-ixP^-} \gamma^+ \langle A | \bar{\chi}(y^-) \mathcal{E}(\theta) \chi(0) | A \rangle, \quad (1)$$

where x is the momentum fraction that initiates a scattering process, meanwhile we measure the energy deposit in a detector at a given angle θ from the initial state radiation and the remnants through the energy operator $\mathcal{E}(\theta) = \lim_{r \rightarrow \infty} \int_0^\infty dt T_{0\bar{n}}(t, \bar{n}r) r^2$ [90–93], $\mathcal{E}(\theta) | X \rangle = \sum_{i \in X} E_i \delta(\theta_i^2 - \theta^2) | X \rangle$. The measured energy deposit is normalized to the energy E_A carried by the nucleus A . Here, χ is the gauge invariant collinear quark field [85–89]. The gluon EEC can be defined similarly. When $\theta E_A \sim \Lambda_{\text{QCD}}$, the f_{EEC} probes the intrinsic transverse dynamics of the nucleus A through the operator $\mathcal{E}(\theta)$.

In the collinear factorization, it has been shown that when $\theta E_A \gg \Lambda_{\text{QCD}}$, the $f_{q,\text{EEC}}(x, \theta)$ can be further factorized as [57]

$$f_{i,\text{EEC}}(x, \theta) = \int \frac{d\xi}{\xi} I_{ij} \left(\frac{x}{\xi}, \theta \right) [\xi f_{j/A}(\xi)], \quad (2)$$

where $f_{j/A}(\xi)$ is the collinear PDF, and I_{ij} is the matching coefficient found to be solely determined by the vacuum collinear splitting functions [57].

As the values of x decreases, the $f_{q,\text{EEC}}$ receives dramatically enhanced contributions from the low x gluon. In this regime, the non-linear small- x dynamics becomes important. Consequently, if compared to the collinear factorization in which the distribution is determined by vacuum collinear splitting, the shape of the θ -distribution will be modified, due to a sizable initial transverse momentum q_t of order the saturation scale Q_s , see, the illustrations in Fig. 1. Therefore, the nucleon EEC can

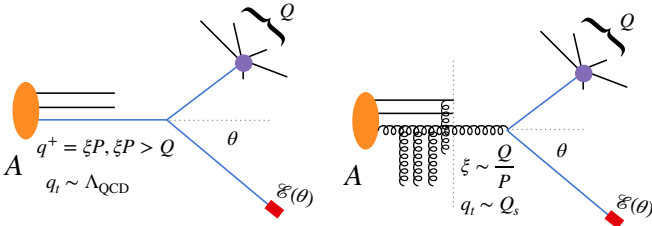


FIG. 1. The $f_{\text{EEC}}(x, \theta)$ in the collinear factorization (left) and the CGC framework (right). Here Q represents the center of mass energy of the partonic cross section.

be used to probe the gluon saturation phenomenon and the small- x dynamics, as we will show in the rest of this manuscript.

The measurement and the factorization theorem. We follow [57] to consider the unpolarized DIS process $l + A \rightarrow l' + X$ in the Breit frame. We assume the nucleus is moving along the $+z$ -direction. We measure the Bjorken $x_B = \frac{-q^2}{2P \cdot q}$, the photon virtuality $Q^2 = -q^2$ and the energy $\sum_i E_i$ that deposits in a calorimeter at an angle θ with respect to the beam, as shown in Fig. 2. Here $q = l' - l$ is the momentum carried by the virtual photon. We then measure the weighted cross section $\Sigma(Q^2, x_B, \theta)$ defined as

$$\Sigma(Q^2, x_B, \theta) = \sum_i \int d\sigma(x_B, Q^2, p_i) \frac{E_i}{E_A} \delta(\theta^2 - \theta_i^2) \quad (3)$$

where E_A is the energy carried by the incoming nucleus. We note that the energy weight suppresses the soft contributions, which is an important feature of the proposed measurement and its resulting nucleon EEC.

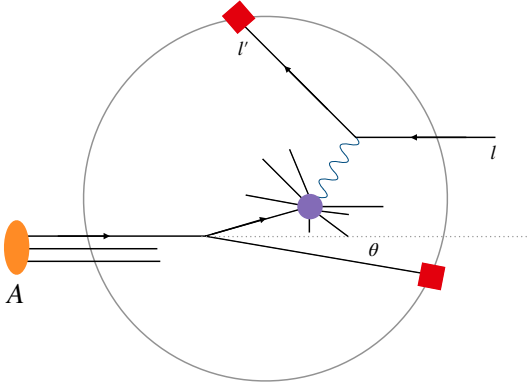


FIG. 2. The x_B and Q^2 measurement in DIS with a forward detector that records the energy flow $\sum_i E_i$ at the angle θ .

In order to probe the small- x dynamics, we are particularly interested in the scenario in which $x_B \ll 0.1$, and we place the detector in the far-forward region such that $Q\theta \ll Q$ while $Q\theta \sim Q_s \gg \Lambda_{\text{QCD}}$. At this point, we emphasize that the measurement involves neither additional

hadron tagging nor jet clustering, and in contrast to the TMD which restricts the events in the small q_t region, this approach is inclusive and does not veto events. It weights the full cross section by the energy recorded at a certain angle θ , therefore the probe is as inclusive as the DIS but with additional control via θ .

When $\theta Q \gg \Lambda_{\text{QCD}}$, the weighted cross section can be calculated perturbatively in the collinear factorization. More interestingly, when $Q\theta \ll Q$, it has been shown that the $\Sigma(Q^2, x_B, \theta)$ fulfils the factorized form [57]

$$\Sigma(Q^2, x_B, \theta) = \int \frac{dx}{x} \hat{\sigma}_{i,\text{DIS}}\left(\frac{x_B}{x}, Q\right) f_{i,\text{EEC}}(x, \theta), \quad (4)$$

where $\hat{\sigma}_{i,\text{DIS}}$ is the fully inclusive partonic DIS cross section. $f_{i,\text{EEC}}$ is the nucleon EEC in Eq. (1). The θ -dependence enters entirely through the nucleon EEC $f_{\text{EEC}}(x, \theta)$, and therefore the θ distribution of the $\Sigma(Q^2, x_B, \theta)$ probes the nucleon EEC when θ is small. We note that f_{EEC} satisfies the same collinear evolution as the collinear PDFs [57]

$$\frac{df_{i,\text{EEC}}(x, \theta)}{d \ln \mu} = P_{ij} \otimes f_{j,\text{EEC}}, \quad (5)$$

as required by $d\Sigma/d \ln \mu = 0$, and since $d\hat{\sigma}_{i,\text{DIS}}/d \ln \mu = -P_{ji} \otimes \hat{\sigma}_{j,\text{DIS}}$. Here the convolution in the momentum fraction is defined as $f \otimes g(x) \equiv \int_x^1 \frac{dz}{z} f\left(\frac{x}{z}\right) g(z)$. It is clear from the evolution that there is no perturbative Sudakov suppression in f_{EEC} , due to the absence of the soft contribution in the collinear factorization eliminated by the energy weight [57].

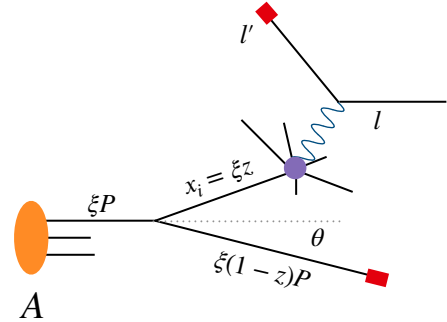


FIG. 3. The collinear splitting that initiates the DIS process and a daughter parton that hits the detector at $\theta \ll 1$. The momentum fractions are shown. We abbreviate P^+ with P in this work for simplicity notation.

The factorization theorem in Eq. (4) and Eq. (2) can be easily understood by considering the leading contribution shown in Fig. 3, where a parton out of the nucleus A with momentum ξP splits into a parton with momentum fraction $(1-z)\xi$ that hits the detector at θ , and an internal line with fraction $z\xi$ and virtuality $t = -\frac{\vec{k}_i^2}{1-z}$ that initiates the partonic inclusive DIS process. Here z is the momentum fraction with respect to the incoming parton

and $k_t = \frac{1}{2}\xi(1-z)P\theta$ is the transverse momentum of the final state parton. In the vacuum, the splitting is described by the leading order vacuum collinear splitting kernel $\frac{1}{t}P_{ij}^{(0)}$. Since $\theta Q \ll Q$, the chance for the radiations from the hard interaction to reach the calorimeter vanishes as $\theta \rightarrow 0$. It is then found that in the small θ limit,

$$\Sigma(Q^2, x_B, \theta) = \int \frac{dx_i}{x_i} \hat{\sigma}_{i,\text{DIS}} \left(Q^2, \frac{x_B}{x_i} \right) \times \int d\xi dz \frac{1}{\theta^2} \delta(x_i - \xi z) (1-z) \xi P_{ij}^{(0)}(z) f_{j/A}(\xi), \quad (6)$$

which, after performing the z integration, gives

$$\Sigma(Q^2, x_B, \theta) = \int \frac{dx_i}{x_i} \hat{\sigma}_{i,\text{DIS}} \left(Q^2, \frac{x_B}{x_i} \right) \times \frac{1}{\theta^2} \int \frac{d\xi}{\xi} \left(1 - \frac{x_i}{\xi} \right) P_{ij}^{(0)} \left(\frac{x_i}{\xi} \right) [\xi f_{j/A}(\xi)]. \quad (7)$$

This produces the factorized form in Eq. (4) and Eq. (2) by identifying the leading order matching coefficient $I_{ij}^{(0)}(\xi, \theta) = \frac{1}{\theta^2} (1-\xi) P_{ij}^{(0)}(\xi)$.

If $x_B \ll 0.1$, the gluon density is overwhelmingly large and the leading contribution to the $\Sigma(Q^2, x_B, \theta)$ is coming from

$$\Sigma(Q^2, x_B, \theta) = \sum_q \frac{4\pi\alpha_s^2 e_q^2}{Q^4} f_{q,\text{EEC}}(x_B, \theta), \quad (8)$$

with

$$f_{q,\text{EEC}}(x, \theta) = \frac{\alpha_s T_R}{2\pi\theta^2} \int_x^1 \frac{d\xi}{\xi} (1-\xi)(\xi^2 + (1-\xi)^2) \left[\frac{x}{\xi} f_g \left(\frac{x}{\xi} \right) \right] \quad (9)$$

The collinear factorization predicts a $\frac{1}{\theta^2}$ -scaling behavior at $\mathcal{O}(\alpha_s)$. For very small θ , the scaling rule could receive corrections from both the evolution of the f_{EEC} in Eq. (5) and non-perturbative effects. But for generic small θ , these effects are mild and therefore $\theta^2 \Sigma$ will be insensitive to the values of θ , up to $\mathcal{O}(\theta Q)$ power corrections. Furthermore, since the energy weight kills the soft contribution, to all orders there will be no perturbative Sudakov suppression in the small θ region in the collinear factorization [57], as is clear from Eq. (5). Such a feature will be modified by the small- x dynamics as we will show.

The nucleon EEC in the small- x regime. In the small- x region, the gluon density grows as $\frac{1}{x}$ and becomes overwhelmingly important and has to be resummed to all orders. To realize such resummation in f_{EEC} , we invoke the CGC effective theory framework and follow the strategy in [94–96] to write the nucleon EEC in terms of the CGC dipole distribution¹. By evaluating the diagrams

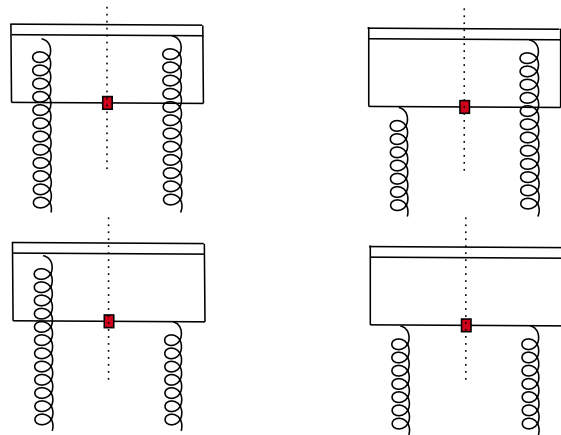


FIG. 4. The leading contribution to $f_{q,\text{EEC}}(x, \theta)$ in the small- x region, where the double line represents the gauge link and the gluon requires momentum $g^+ = x_g P$ and $g_t \sim Q_s \sim \theta Q$.

in Fig. 4, we find in the leading logarithmic (LL) approximation

$$f_{q,\text{EEC}}(x_B, \theta) = \frac{N_C S_\perp}{8\pi^4} \int d^2 \vec{g}_t \times \int_{\xi_{\text{cut}}}^1 \frac{d\xi}{\xi} \mathcal{A}_{qg}(\xi, \theta, \vec{g}_t) F_{g,x_B}(\vec{g}_t), \quad (10)$$

where S_\perp is the averaged transverse area of the target nucleus and $g_t \sim Q_s \sim \theta Q$ is the transverse momentum transfer. $F_{g,x_F} = \int \frac{d^2 \vec{r}_t}{4\pi^2} e^{-i\vec{g}_t \cdot \vec{r}_t} S_{x_F}^{(2)}(\vec{r}_t)$ is the CGC dipole distribution evaluated at the scale x_F , where $S_{x_F}^{(2)}(\vec{r}_t) = \frac{1}{N_C} \langle \text{Tr}[W(\vec{r}_t)W^\dagger(\vec{0})] \rangle_{x_F}$. $x_F \frac{Q}{x_B}$ is the rapidity scale/boundary that separates the fast moving modes being integrated out and the active slow moving partons in the CGC effective framework. In this work, we default to the natural choice $x_F = x_B$. $\frac{1-\xi}{\xi} Q$ is the momentum “+”-component that enters the detector. ξ_{cut} is determined by requiring the momentum of the active quark does not exceed the rapidity boundary. Here the coefficient \mathcal{A}_{qg} is given by

$$\mathcal{A}_{qg}(\xi, \theta, \vec{g}_t) = \frac{1}{\theta^2} (1-\xi) \vec{k}_t^2 (\vec{k}_t - \vec{g}_t)^2 \times \left| \frac{\vec{k}_t}{\xi \vec{k}_t^2 + (1-\xi)(\vec{k}_t - \vec{g}_t)^2} - \frac{\vec{k}_t - \vec{g}_t}{(\vec{k}_t - \vec{g}_t)^2} \right|^2, \quad (11)$$

with k_t defined as $k_t = \frac{1-\xi}{\xi} \frac{Q}{2} \theta$, should be of order Q_s .

It is easy to show that if $g_t \sim Q_s \ll \theta Q$, Eq. (10) reduces to the $\frac{1}{\theta^2}$ -scaling behavior of the collinear factorization in Eq. (9). On the other hand, if $\theta Q \ll Q_s$,

¹ The complete calculation using the full dipole amplitude $\psi_{T,L}^{\gamma^* \rightarrow q\bar{q}}$

for $\gamma^* \rightarrow q\bar{q}$ is presented in the Supplemental Material. Both approaches agree in the small θ limit.

Eq. (10) scales as θ^0 . We thus expect that in CGC, the $\theta^2\Sigma$ will be independent of the θ for $\theta Q \gg Q_s$, however, contrary to the collinear factorization, suppressed when $\theta Q \ll Q_s$. Meanwhile the θ region between these two limits provide the opportunity to estimate the saturation scale Q_s .

Numerics. Now we study the numerical impacts of the small- x dynamics on the shape of the $\theta^2\Sigma(Q^2, x_B, \theta)$ distribution from Eq. (10), compared with the collinear prediction. We are particularly interested in the region $\theta \ll 1$ where the θ distribution probes directly the $f_{\text{EEC}}(x, \theta)$, see Eq. (4). For the small- x dipole distribution $S_{x_F}^{(2)}(\vec{r}_t)$, we use both the MV model with rcBK running [12, 13, 18, 97–104] and the GBW model [105].

As for the MV model with rcBK running, we adopt

the MV-like model [106] as the initial condition, whose form is $S_{x_0}^{(2)}(\vec{r}_t) = \exp\left[-\frac{(r_t^2 Q_{s0}^2)^\gamma}{4} \ln\left(\frac{1}{\Lambda r_t} + e\right)\right]$, where we choose $x_0 = 0.01$, $\gamma = 1.119$, $\Lambda = 0.241$ GeV, $Q_{s0}^2 = A^{1/3} 0.168$ GeV² with A the atomic number. We use the solution to the LL BK evolution with α_s running [98, 101, 106] of the dipole distribution to evolve the dipole distribution from x_0 to x_F . In our calculation, we use the result fitted from the HERA data for the transverse area of the nucleus S_\perp [19]. The GBW model is implemented using $S_{x_F}^{(2)}(\vec{r}_t) = \exp\left[-\frac{1}{4} r_t^2 Q_s^2(x_F)\right]$, where $Q_s^2(x_F) = A_N (x_0/x_F)^\lambda$ GeV² and we use $x_0 = 2.24 \times 10^{-4}$, $\lambda = 0.27$ and $A_N = 1$ for the proton while $A_N = 5$ for the Au [107].

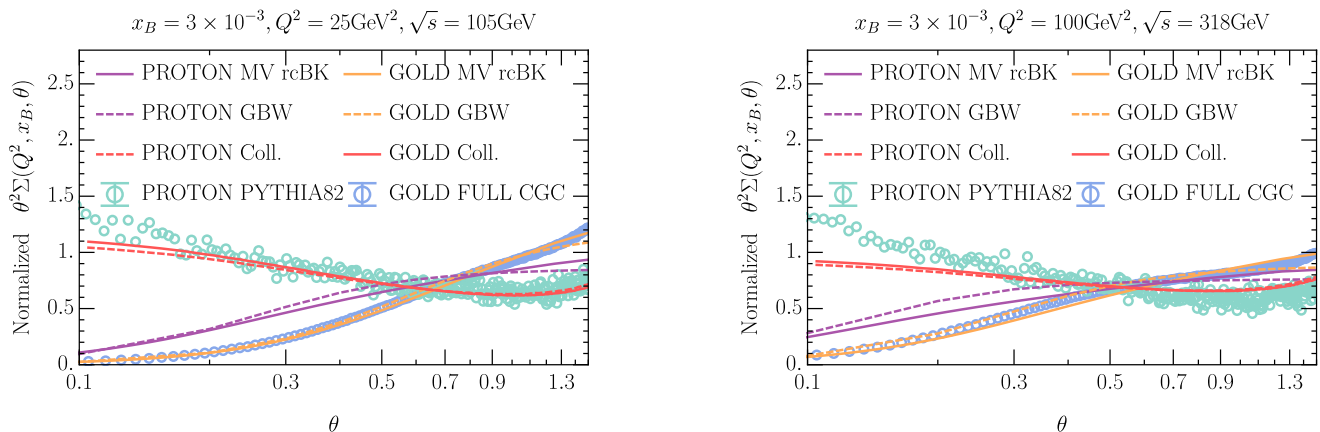


FIG. 5. Normalized $\theta^2\Sigma(Q^2, x_B, \theta)$ distribution for proton and Au, with $x_B = 0.003$, for both $Q^2 = 25$ GeV², $\sqrt{s} = 105$ GeV (left panel) and $Q^2 = 100$ GeV², $\sqrt{s} = 318$ GeV (right panel). Green dots are from `Pythia82` simulation, in which we demand $0.00295 < x_B < 0.00305$, and $25\text{GeV}^2 \leq Q^2 < 35\text{GeV}^2$ for the left panel while $100\text{GeV}^2 \leq Q^2 < 110\text{GeV}^2$ for the right.

In Fig. 5, we show the CGC predictions for $\theta^2\Sigma(Q^2, x_B, \theta)$ as a function of θ . Since we are only interested in the shape, we normalized the distribution by $\int_{\theta_{\min}}^{\theta_{\max}} d\theta \theta^2 \Sigma$. We fixed $x_B = 3 \times 10^{-3}$ and choose $Q^2 = 25$ GeV², $\sqrt{s} = 105$ GeV (left panel) and $Q^2 = 100$ GeV², $\sqrt{s} = 318$ GeV (right panel). We present predictions from CGC for both proton (in purple lines) and Au (in orange), by the MV model with rcBK running and GBW model. We see both models predict similar shapes in the θ spectrum, in which the small- θ region is suppressed. They are impressively different from the collinear expectations (in red lines and green dots). In the figure, the collinear predictions (red lines) are made out of the complete fixed order α_s calculation, without the $Q\theta \ll Q$ approximation, using `CT18A` [108] and `EPPS21` [109] PDF sets for proton and Au, respectively. To validate our collinear calculation and to estimate the size of the evolution effect in Eq. (5), we also run a `Pythia82` simu-

lation [110] for the proton case, where the LL resummation is performed. We see that for large θ , the fixed order calculations agree well with the the `Pythia` simulation, while for small θ values, the resummation effects could be sizable but does not suppress the small- θ region due to the absence of the perturbative Sudakov factor in f_{EEC} in the collinear factorization. The collinear prediction for the Au follows closely the proton's. The notable difference demonstrates that the $f_{\text{EEC}}(x, \theta)$ could serve as a clean probe of the small- x phenomenon. For comparison, we also show the predictions from the full CGC calculation derived in the Supplemental Material using the GBW model in purple circles.

In Fig. 5, the proton spectrum turns into a plateau for large values of θ , which is expected from Eq. (10) when $Q\theta \gg Q_s$. We can define a turning point around which the slope of the distribution starts to switch its monotonicity. The turning point allows us to estimate the size of the saturation scale Q_s . For instance, from

the left panel of Fig. 5, the turning point for the proton is roughly around $\theta \sim 0.15-0.2$ and thus $Q_s \sim \theta Q \sim 0.75-1.0$ GeV which is consistent with the values of Λ_{QCD} . And we estimate the saturation scale for the Au will be around $\theta \sim 0.4-0.5$ and thus $Q_s \sim \theta Q \sim 2-2.5$ GeV. The right panel of Fig. 5 is similar to the left, but with $Q^2 = 100 \text{ GeV}^2$. Since Q^2 is larger, the distribution enters the plateau earlier as expected. Now the turning point for the Au is around $\theta \sim 0.2-0.3$ which again indicates that $Q_s \sim 2-3$ GeV, consistent with the $Q^2 = 25 \text{ GeV}^2$ case.

We can further introduce the nuclear modification factor $R_{pA} = \frac{A^{-1} \Sigma_A(Q^2, x_B, \theta)}{\Sigma_p(Q^2, x_B, \theta)}$, which helps to reduce the systematics. In the collinear factorization, for $\theta Q \gg \Lambda_{\text{QCD}}$, the θ distribution is determined by the matching coefficient I_{ij} as predicted by Eq. (8), which is independent of the incoming nucleus species. Thus taking the ratio R_{Ap} reduces the impacts from perturbative higher order corrections as well as possible non-perturbative hadronization effects, and the collinear factorization predicts the R_{Ap} insensitive to the θ values, as showed explicitly as red lines in Fig. 6.

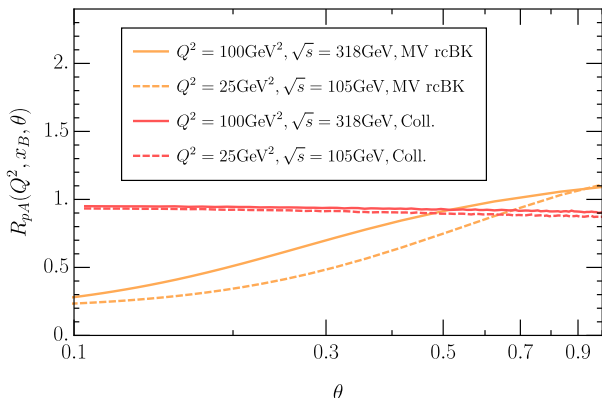


FIG. 6. R_{pA} as a function of θ , with $x_B = 3 \times 10^{-3}$ using the MV model with rcBK running and collinear factorization.

Once again, the small- x formalism changes the pattern as we observed in Fig. 6, where the modification factor R_{pA} is suppressed in the small θ region, while converges toward around unity as θ becomes large and $Q\theta \gg Q_s$.

Conclusions. In this manuscript, we have proposed the nucleon energy-energy correlator (nucleon EEC) as a new probe of the gluon saturation phenomenon in DIS at the future electron-ion colliders. In particular, we have shown that the θ -shape of the nucleon EEC $f_{\text{EEC}}(x, \theta)$ behaves differently in the collinear factorization theorem and the CGC formalism. The drastic difference is due to the intrinsic transverse momentum of order Q_s induced by the non-linear small- x dynamics. We thus expect the f_{EEC} to complement the other standard small- x processes and offer a great opportunity to pin down the onset of the gluon saturation phenomenon in eA -collisions.

The advantage of the nucleon EEC probe, as compared to other standard small- x processes, is that it is fully inclusive, involving no fragmentation functions and jet clustering. Therefore the observable is expected to be clean both theoretically and experimentally. Extensions to other observables that are induced by the intrinsic transverse dynamics of the nucleon/nucleus shall follow. For polarized hadron beam, we can study the spin asymmetry by adding the azimuthal dependence to the energy operator \mathcal{E} and we expect different asymmetries to be predicted in the collinear and CGC frameworks. We hope that the results presented in this manuscript will motivate carrying out the proposed measurement at the current and future electron-ion facilities, meanwhile stimulate further applications of the nucleon EEC in nuclear structure studies.

Acknowledgement. We are grateful to Farid Salazar, Hongxi Xing, Jian Zhou for useful discussions. This work is supported by the Natural Science Foundation of China under contract No. 12175016 (X. L.), No. 11975200 (H. X. Z.), and the Office of Science of the U.S. Department of Energy under Contract No. DE-AC02-05CH11231 (F.Y.).

* xiliu@bnu.edu.cn

† fyuan@lbl.gov

‡ zhuhx@zju.edu.cn

- [1] L. V. Gribov, E. M. Levin, and M. G. Ryskin, Phys. Rept. **100**, 1 (1983).
- [2] A. H. Mueller and J.-w. Qiu, Nucl. Phys. B **268**, 427 (1986).
- [3] A. H. Mueller, Nucl. Phys. B **335**, 115 (1990).
- [4] L. D. McLerran and R. Venugopalan, Phys. Rev. D **49**, 2233 (1994), hep-ph/9309289.
- [5] L. D. McLerran and R. Venugopalan, Phys. Rev. D **49**, 3352 (1994), hep-ph/9311205.
- [6] L. D. McLerran and R. Venugopalan, Phys. Rev. D **50**, 2225 (1994), hep-ph/9402335.
- [7] A. Accardi *et al.*, Eur. Phys. J. A **52**, 268 (2016), 1212.1701.
- [8] R. Abdul Khalek *et al.*, (2021), 2103.05419.
- [9] *Proceedings, Probing Nucleons and Nuclei in High Energy Collisions: Dedicated to the Physics of the Electron Ion Collider: Seattle (WA), United States, October 1 - November 16, 2018*, WSP, 2020, 2002.12333.
- [10] F. Gelis, E. Iancu, J. Jalilian-Marian, and R. Venugopalan, Ann. Rev. Nucl. Part. Sci. **60**, 463 (2010), 1002.0333.
- [11] E. Iancu and R. Venugopalan, *The Color glass condensate and high-energy scattering in QCD* (, 2003), pp. 249-3363, hep-ph/0303204.
- [12] I. Balitsky, Nucl. Phys. B **463**, 99 (1996), hep-ph/9509348.
- [13] Y. V. Kovchegov, Phys. Rev. D **60**, 034008 (1999), hep-ph/9901281.
- [14] J. Jalilian-Marian, A. Kovner, A. Leonidov, and H. Weigert, Nucl. Phys. B **504**, 415 (1997), hep-

- ph/9701284.
- [15] J. Jalilian-Marian, A. Kovner, A. Leonidov, and H. Weigert, *Phys. Rev. D* **59**, 014014 (1998), hep-ph/9706377.
- [16] E. Iancu, A. Leonidov, and L. D. McLerran, *Nucl. Phys. A* **692**, 583 (2001), hep-ph/0011241.
- [17] E. Ferreira, E. Iancu, A. Leonidov, and L. McLerran, *Nucl. Phys. A* **703**, 489 (2002), hep-ph/0109115.
- [18] J. L. Albacete, N. Armesto, J. G. Milhano, P. Quiroga-Arias, and C. A. Salgado, *Eur. Phys. J. C* **71**, 1705 (2011), 1012.4408.
- [19] T. Lappi and H. Mäntysaari, *Phys. Rev. D* **88**, 114020 (2013), 1309.6963.
- [20] B. Ducloué, H. Hänninen, T. Lappi, and Y. Zhu, *Phys. Rev. D* **96**, 094017 (2017), 1708.07328.
- [21] F. Dominguez, B.-W. Xiao, and F. Yuan, *Phys. Rev. Lett.* **106**, 022301 (2011), 1009.2141.
- [22] F. Dominguez, C. Marquet, B.-W. Xiao, and F. Yuan, *Phys. Rev. D* **83**, 105005 (2011), 1101.0715.
- [23] A. H. Mueller, B.-W. Xiao, and F. Yuan, *Phys. Rev. D* **88**, 114010 (2013), 1308.2993.
- [24] A. Metz and J. Zhou, *Phys. Rev. D* **84**, 051503 (2011), 1105.1991.
- [25] F. Dominguez, J.-W. Qiu, B.-W. Xiao, and F. Yuan, *Phys. Rev. D* **85**, 045003 (2012), 1109.6293.
- [26] A. Dumitru, T. Lappi, and V. Skokov, *Phys. Rev. Lett.* **115**, 252301 (2015), 1508.04438.
- [27] A. Dumitru and V. Skokov, *Phys. Rev. D* **94**, 014030 (2016), 1605.02739.
- [28] D. Boer, P. J. Mulders, C. Pisano, and J. Zhou, *JHEP* **08**, 001 (2016), 1605.07934.
- [29] G. Beuf, *Phys. Rev. D* **96**, 074033 (2017), 1708.06557.
- [30] A. Dumitru, V. Skokov, and T. Ullrich, *Phys. Rev. C* **99**, 015204 (2019), 1809.02615.
- [31] H. Mäntysaari, N. Mueller, F. Salazar, and B. Schenke, *Phys. Rev. Lett.* **124**, 112301 (2020), 1912.05586.
- [32] Y.-Y. Zhao, M.-M. Xu, L.-Z. Chen, D.-H. Zhang, and Y.-F. Wu, *Phys. Rev. D* **104**, 114032 (2021), 2105.08818.
- [33] R. Boussarie, H. Mäntysaari, F. Salazar, and B. Schenke, *JHEP* **09**, 178 (2021), 2106.11301.
- [34] P. Caucal, F. Salazar, and R. Venugopalan, *JHEP* **11**, 222 (2021), 2108.06347.
- [35] Y.-Y. Zhang and X.-N. Wang, *Phys. Rev. D* **105**, 034015 (2022), 2104.04520.
- [36] P. Taels, T. Altinoluk, G. Beuf, and C. Marquet, *JHEP* **10**, 184 (2022), 2204.11650.
- [37] P. Caucal, F. Salazar, B. Schenke, and R. Venugopalan, *JHEP* **11**, 169 (2022), 2208.13872.
- [38] R. Boussarie, A. V. Grabovsky, L. Szymanowski, and S. Wallon, *JHEP* **09**, 026 (2014), 1405.7676.
- [39] R. Boussarie, A. V. Grabovsky, L. Szymanowski, and S. Wallon, *JHEP* **11**, 149 (2016), 1606.00419.
- [40] F. Salazar and B. Schenke, *Phys. Rev. D* **100**, 034007 (2019), 1905.03763.
- [41] R. Boussarie, A. V. Grabovsky, L. Szymanowski, and S. Wallon, *Phys. Rev. D* **100**, 074020 (2019), 1905.07371.
- [42] D. Boer and C. Setyadi, *Phys. Rev. D* **104**, 074006 (2021), 2106.15148.
- [43] E. Iancu, A. H. Mueller, and D. N. Triantafyllopoulos, *Phys. Rev. Lett.* **128**, 202001 (2022), 2112.06353.
- [44] E. Iancu, A. H. Mueller, D. N. Triantafyllopoulos, and S. Y. Wei, *JHEP* **10**, 103 (2022), 2207.06268.
- [45] Y. Hatta, B.-W. Xiao, and F. Yuan, *Phys. Rev. Lett.* **116**, 202301 (2016), 1601.01585.
- [46] T. Altinoluk, N. Armesto, G. Beuf, and A. H. Rezaeian, *Phys. Lett. B* **758**, 373 (2016), 1511.07452.
- [47] H. Mäntysaari, N. Mueller, and B. Schenke, *Phys. Rev. D* **99**, 074004 (2019), 1902.05087.
- [48] Y. Hagiwara, C. Zhang, J. Zhou, and Y.-j. Zhou, *Phys. Rev. D* **104**, 094021 (2021), 2106.13466.
- [49] L. Zheng, E. C. Aschenauer, J. H. Lee, and B.-W. Xiao, *Phys. Rev. D* **89**, 074037 (2014), 1403.2413.
- [50] F. Bergabo and J. Jalilian-Marian, *Nucl. Phys. A* **1018**, 122358 (2022), 2108.10428.
- [51] F. Bergabo and J. Jalilian-Marian, *Phys. Rev. D* **106**, 054035 (2022), 2207.03606.
- [52] E. Iancu and Y. Mulian, (2022), 2211.04837.
- [53] M. Fucilla, A. V. Grabovsky, E. Li, L. Szymanowski, and S. Wallon, (2022), 2211.05774.
- [54] I. Kolbé, K. Roy, F. Salazar, B. Schenke, and R. Venugopalan, *JHEP* **01**, 052 (2021), 2008.04372.
- [55] X.-B. Tong, B.-W. Xiao, and Y.-Y. Zhang, (2022), 2211.01647.
- [56] T. Altinoluk, G. Beuf, A. Czajka, and A. Tymowska, (2022), 2212.10484.
- [57] X. Liu and H. X. Zhu, (2022), 2209.02080.
- [58] C. Basham, L. S. Brown, S. D. Ellis, and S. T. Love, *Phys. Rev. Lett.* **41**, 1585 (1978).
- [59] C. Basham, L. Brown, S. Ellis, and S. Love, *Phys. Rev. D* **19**, 2018 (1979).
- [60] H. Chen, I. Moulton, X. Zhang, and H. X. Zhu, *Phys. Rev. D* **102**, 054012 (2020), 2004.11381.
- [61] D. M. Hofman and J. Maldacena, *JHEP* **05**, 012 (2008), 0803.1467.
- [62] A. Belitsky, S. Hohenegger, G. Korchemsky, E. Sokatchev, and A. Zhiboedov, *Phys. Rev. Lett.* **112**, 071601 (2014), 1311.6800.
- [63] A. Belitsky, S. Hohenegger, G. Korchemsky, E. Sokatchev, and A. Zhiboedov, *Nucl. Phys. B* **884**, 305 (2014), 1309.0769.
- [64] M. Kologlu, P. Kravchuk, D. Simmons-Duffin, and A. Zhiboedov, *JHEP* **01**, 128 (2021), 1905.01311.
- [65] G. Korchemsky, *JHEP* **01**, 008 (2020), 1905.01444.
- [66] L. J. Dixon, I. Moulton, and H. X. Zhu, *Phys. Rev. D* **100**, 014009 (2019), 1905.01310.
- [67] H. Chen *et al.*, *JHEP* **08**, 028 (2020), 1912.11050.
- [68] H. Chen, I. Moulton, and H. X. Zhu, *Phys. Rev. Lett.* **126**, 112003 (2021), 2011.02492.
- [69] C.-H. Chang, M. Kologlu, P. Kravchuk, D. Simmons-Duffin, and A. Zhiboedov, *JHEP* **05**, 059 (2022), 2010.04726.
- [70] Y. Li, I. Moulton, S. S. van Velzen, W. J. Waalewijn, and H. X. Zhu, *Phys. Rev. Lett.* **128**, 182001 (2022), 2108.01674.
- [71] M. Jaarsma, Y. Li, I. Moulton, W. Waalewijn, and H. X. Zhu, *JHEP* **06**, 139 (2022), 2201.05166.
- [72] P. T. Komiske, I. Moulton, J. Thaler, and H. X. Zhu, (2022), 2201.07800.
- [73] J. Holguin, I. Moulton, A. Pathak, and M. Procura, (2022), 2201.08393.
- [74] K. Yan and X. Zhang, *Phys. Rev. Lett.* **129**, 021602 (2022), 2203.04349.
- [75] H. Chen, I. Moulton, J. Sandor, and H. X. Zhu, (2022), 2202.04085.
- [76] C.-H. Chang and D. Simmons-Duffin, (2022), 2202.04090.

- [77] H. Chen, I. Moulton, J. Thaler, and H. X. Zhu, *JHEP* **07**, 146 (2022), 2205.02857.
- [78] K. Lee, B. Meçaj, and I. Moulton, (2022), 2205.03414.
- [79] A. J. Larkoski, (2022), 2205.12375.
- [80] L. Ricci and M. Riemann, (2022), 2207.03511.
- [81] T.-Z. Yang and X. Zhang, (2022), 2208.01051.
- [82] C. Andres *et al.*, (2022), 2209.11236.
- [83] H. Chen *et al.*, (2022), 2210.10058.
- [84] E. Craft, K. Lee, B. Meçaj, and I. Moulton, (2022), 2210.09311.
- [85] C. W. Bauer, S. Fleming, D. Pirjol, and I. W. Stewart, *Phys. Rev. D* **63**, 114020 (2001), hep-ph/0011336.
- [86] C. W. Bauer, D. Pirjol, and I. W. Stewart, *Phys. Rev. D* **65**, 054022 (2002), hep-ph/0109045.
- [87] C. W. Bauer and I. W. Stewart, *Phys. Lett. B* **516**, 134 (2001), hep-ph/0107001.
- [88] M. Beneke, A. P. Chapovsky, M. Diehl, and T. Feldmann, *Nucl. Phys. B* **643**, 431 (2002), hep-ph/0206152.
- [89] C. W. Bauer, S. Fleming, D. Pirjol, I. Z. Rothstein, and I. W. Stewart, *Phys. Rev. D* **66**, 014017 (2002), hep-ph/0202088.
- [90] N. A. Sveshnikov and F. V. Tkachov, *Phys. Lett. B* **382**, 403 (1996), hep-ph/9512370.
- [91] F. V. Tkachov, *Int. J. Mod. Phys. A* **12**, 5411 (1997), hep-ph/9601308.
- [92] G. P. Korchemsky and G. F. Sterman, *Nucl. Phys. B* **555**, 335 (1999), hep-ph/9902341.
- [93] C. W. Bauer, S. P. Fleming, C. Lee, and G. F. Sterman, *Phys. Rev. D* **78**, 034027 (2008), 0801.4569.
- [94] C. Marquet, B.-W. Xiao, and F. Yuan, *Phys. Lett. B* **682**, 207 (2009), 0906.1454.
- [95] B.-W. Xiao, F. Yuan, and J. Zhou, *Nucl. Phys. B* **921**, 104 (2017), 1703.06163.
- [96] J. Zhou, *Phys. Rev. D* **99**, 054026 (2019), 1807.00506.
- [97] Y. V. Kovchegov and H. Weigert, *Nucl. Phys. A* **789**, 260 (2007), hep-ph/0612071.
- [98] Y. V. Kovchegov and H. Weigert, *Nucl. Phys. A* **784**, 188 (2007), hep-ph/0609090.
- [99] K. J. Golec-Biernat, L. Motyka, and A. M. Stasto, *Phys. Rev. D* **65**, 074037 (2002), hep-ph/0110325.
- [100] J. L. Albacete and Y. V. Kovchegov, *Phys. Rev. D* **75**, 125021 (2007), 0704.0612.
- [101] I. Balitsky, *Phys. Rev. D* **75**, 014001 (2007), hep-ph/0609105.
- [102] E. Gardi, J. Kuokkanen, K. Rummukainen, and H. Weigert, *Nucl. Phys. A* **784**, 282 (2007), hep-ph/0609087.
- [103] I. Balitsky and G. A. Chirilli, *Phys. Rev. D* **77**, 014019 (2008), 0710.4330.
- [104] J. Berger and A. Stasto, *Phys. Rev. D* **83**, 034015 (2011), 1010.0671.
- [105] K. J. Golec-Biernat and M. Wusthoff, *Phys. Rev. D* **59**, 014017 (1998), hep-ph/9807513.
- [106] H. Fujii and K. Watanabe, *Nucl. Phys. A* **915**, 1 (2013), 1304.2221.
- [107] K. Golec-Biernat and S. Sapeta, *JHEP* **03**, 102 (2018), 1711.11360.
- [108] T.-J. Hou *et al.*, *Phys. Rev. D* **103**, 014013 (2021), 1912.10053.
- [109] K. J. Eskola, P. Paakkinen, H. Paukkunen, and C. A. Salgado, *Eur. Phys. J. C* **82**, 413 (2022), 2112.12462.
- [110] T. Sjöstrand *et al.*, *Comput. Phys. Commun.* **191**, 159 (2015), 1410.3012.

Supplemental Materials for “Nucleon Energy Correlators for the Color Glass Condensate”

Hao-Yu Liu,¹ Xiaohui Liu,^{1,*} Ji-Chen Pan,^{2,3} Feng Yuan,^{4,†} and Hua Xing Zhu^{5,‡}

¹*Center of Advanced Quantum Studies, Department of Physics,
Beijing Normal University, Beijing, 100875, China*

²*Institute of High Energy Physics, Chinese Academy of Sciences, Beijing 100049, China*

³*School of Physics, University of Chinese Academy of Sciences, Beijing 100049, China*

⁴*Nuclear Science Division, Lawrence Berkeley National Laboratory, Berkeley, CA 94720, USA*

⁵*Zhejiang Institute of Modern Physics, Department of Physics, Zhejiang University, Hangzhou, 310027, China*
(Dated: January 3, 2023)

Here we present the $\Sigma(Q^2, x_B, \theta)$

$$\Sigma(Q^2, x_B, \theta) = \sum_i \int d\sigma(x_B, Q^2, p_i) \frac{E_i}{E_A} \delta(\theta^2 - \theta_i^2), \quad (1)$$

within the CGC formalism without the small θ approximation. The calculation is achieved by evaluating amplitude for a virtual photon γ^* splitting into the $q\bar{q}$ pair, as shown in Fig. 1. Each of the quarks will enter the detector to contribute to the energy deposit E_i , which we assume it is always the \bar{q} . The contribution from the q is obtained by multiplying a symmetric factor at this order.

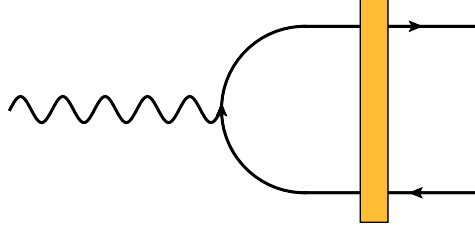


FIG. 1. Dipole amplitude for $\gamma^* \rightarrow q\bar{q}$. The orange block represents the CGC Wilson line.

We work in the Breit frame, in which $q = (0, 0, 0, -Q)$ for the virtual photon, and $P = \frac{Q}{2x_B}(1, 0, 0, 1)$ for the nucleus. The calculation is straightforward which gives

$$\Sigma(Q^2, x_B, \theta) = \sum_{\lambda=l,t} f_\lambda \Sigma_\lambda^{\gamma^*}(Q^2, x_B, \theta), \quad (2)$$

where we sum over the virtual photon polarization with the flux $f_t = 1 - y + \frac{y^2}{2}$ for the transverse and $f_l = 1 - y$ longitudinal polarization, respectively, with $y = \frac{Q^2}{x_B s}$ the inelasticity. Here for the transverse photon contribution, we find

$$\begin{aligned} \Sigma_t^{\gamma^*}(Q^2, x_B, \theta) &= \sum_q \frac{2N_c \alpha^2 e_q^2}{\pi^2 x_B Q^2} S_\perp \int dz d^2 \vec{k}_t \frac{d^2 \vec{l}_t}{(2\pi)^2} F_{g,x_B}(\vec{l}_t) [z^2 + (1-z)^2] \left| \frac{\vec{k}_t}{\vec{k}_t^2 + \Delta^2} - \frac{\vec{k}_t - \vec{l}_t}{(\vec{k}_t - \vec{l}_t)^2 + \Delta^2} \right|^2 \\ &\times \left[\frac{\vec{k}_t^2 + (1-z)^2 Q^2}{(1-z)Q} \frac{x_B}{Q} \right] \frac{1}{2\theta} \delta \left(\theta - \tan^{-1} \frac{2k_t(1-z)Q}{k_t^2 - (1-z)^2 Q^2} \right) \theta \left(\frac{\vec{k}_t^2 + (1-z)^2 Q^2}{(1-z)Q} < x_B \frac{Q}{x_B} \right), \quad (3) \end{aligned}$$

where k is the momentum for \bar{q} and $1-z = \frac{k^-}{Q}$ the momentum fraction with respect to the photon. We defined $\Delta^2 = z(1-z)Q^2$. In the last line, the first term is the energy weight, derived using the on-shell condition $k^+ k^- - \vec{k}_t^2 = 0$, normalized to the incoming nucleus energy Q/x_B in the Breit frame. The second term defines the θ angle with respect

* xiliu@bnu.edu.cn

† fyuan@lbl.gov

‡ zhuhx@zju.edu.cn

to the z -axis, with $\theta < \pi/2$ for $k_z > 0$ while $\theta > \pi/2$ for $k_z < 0$. The last θ function ensures that $2k^0$ can not exceed the incoming parton momentum $x_B P = x_B \frac{Q}{x_B}$ [1]. As for the longitudinal polarization, we have

$$\begin{aligned} \Sigma_l^{\gamma^*}(Q^2, x_B, \theta) &= \sum_q \frac{2N_c \alpha^2 e_q^2}{\pi^2 x_B Q^2} S_\perp \int dz d^2 \vec{k}_t \frac{d^2 \vec{l}_t}{(2\pi)^2} F_{g, x_B}(\vec{l}_t) 4z^2 (1-z)^2 Q^2 \left| \frac{1}{\vec{k}_t^2 + \Delta^2} - \frac{1}{(\vec{k}_t - \vec{l}_t)^2 + \Delta^2} \right|^2 \\ &\times \left[\frac{\vec{k}_t^2 + (1-z)^2 Q^2}{(1-z)Q} \frac{x_B}{Q} \right] \frac{1}{2\theta} \delta \left(\theta - \tan^{-1} \frac{2k_t(1-z)Q}{k_t^2 - (1-z)^2 Q^2} \right) \theta \left(\frac{\vec{k}_t^2 + (1-z)^2 Q^2}{(1-z)Q} < x_B \frac{Q}{x_B} \right). \end{aligned} \quad (4)$$

Now we consider the small- θ limit. As $\theta \rightarrow 0$, the contribution is dominated by $1-z \sim \frac{k_t^2}{Q^2}$. We define the variable ξ through $(1-z)Q = \frac{\xi}{1-\xi} \frac{k_t^2}{Q}$ and only keep the leading contribution in $z \rightarrow 1$ limit to find

$$\begin{aligned} \Sigma(Q^2, x_B, \theta) &= \sum_q \frac{4\pi \alpha^2 e_q^2}{Q^4} \frac{N_c S_\perp}{8\pi^4} \frac{1}{\theta^2} \int \frac{d\xi}{\xi} d^2 \vec{l}_t (1-\xi) k_t^2 (k_t - l_t)^2 \left| \frac{\vec{k}_t}{\xi \vec{k}_t^2 + (1-\xi)(\vec{k}_t - \vec{l}_t)^2} - \frac{\vec{k}_t - \vec{l}_t}{(\vec{k}_t - \vec{l}_t)^2} \right|^2 \\ &\times \theta \left(\frac{1-\xi}{\xi} < 1 \right) F_{g, x_B}(\vec{l}_t), \end{aligned} \quad (5)$$

where $k_t = \frac{1-\xi}{\xi} \frac{Q}{2}$. We thus identify $f_{\text{EEC}}(x_B, \theta)$ at this order in the small- x formalism as

$$f_{q, \text{EEC}}(x_B, \theta) = \frac{N_c S_\perp}{8\pi^4} \frac{1}{\theta^2} \int_{\xi_{\text{cut}}}^1 \frac{d\xi}{\xi} d^2 \vec{l}_t (1-\xi) k_t^2 (k_t - l_t)^2 \left| \frac{\vec{k}_t}{\xi \vec{k}_t^2 + (1-\xi)(\vec{k}_t - \vec{l}_t)^2} - \frac{\vec{k}_t - \vec{l}_t}{(\vec{k}_t - \vec{l}_t)^2} \right|^2 F_{g, x_B}(\vec{l}_t). \quad (6)$$

The ξ_{cut} is determined from the last θ -function in Eq. (5).

[1] G. Beuf, Phys. Rev. D **96**, 074033 (2017), 1708.06557.